Numerical modelling of high-pressure arc discharges: matching the LTE arc core with the electrodes

IOP Publishing Journal of Physics D: Applied Physics
J. Phys. D: Appl. Phys. **50** (2017) 315203 (9pp) https://doi.org/10.1088/1361-6463/aa76d3

Numerical modelling of high-pressure arc discharges: matching the LTE arc core with the electrodes

M Lisnyak[1,4], M D Cunha[2,3], J-M Bauchire[1] and M S Benilov[2,3,4]

[1] GREMI, UMR 7344, CNRS/Université d'Orléans, 14 Rue d'Issoudun, Orléans 45067, France
[2] Departamento de Física, FCEE, Universidade da Madeira, Largo do Município, 9000 Funchal, Portugal
[3] Instituto de Plasmas e Fusão Nuclear, IST, Universidade de Lisboa, 1649-004 Lisboa, Portugal

E-mail: marina.lisnyak@univ-orleans.fr, benilov@uma.pt

Received 27 March 2017, revised 4 May 2017
Accepted for publication 2 June 2017
Published 17 July 2017

Abstract

A widely used approach to simulation of high-pressure arc discharges is based on the system of magneto-hydrodynamic equations written in the approximation of local thermodynamic equilibrium (LTE). In this work, boundary conditions on the surface of the electrodes are formulated with the use of equations of balance of energy in the non-equilibrium near-electrode layers that separate the LTE bulk plasma and the electrodes. As an example, numerical simulations of a free-burning arc in atmospheric-pressure argon plasma in the current range from 20 to 200 A are reported. Simulation results are in reasonably good agreement with those given by more sophisticated models and with the experiment. Simulations performed for cathodes of slightly different geometries have predicted a strong effect produced by details of the cathode geometry over the distribution of the current density along the cathode surface and therefore over the plasma temperature, an interesting and potentially important result that is worth further numerical investigation and experimental verification.

Keywords: high-pressure arcs, arc-electrodes interaction, LTE arc core description, matching conditions with electrodes

(Some figures may appear in colour only in the online journal)

1. Introduction

Numerical modelling of high-pressure electric arc discharges is of high interest due to many industrial applications [1, 2]. The essential elements of the numerical models are boundary conditions on interfaces separating the bulk plasma from the electrodes, which are supposed to provide a reasonably accurate description of the physics governing the plasma–electrode interaction.

Formulation of these boundary conditions depends on the description of the bulk plasma being used; see discussion in [3] and references therein. If the bulk plasma is described by means of a fully non-equilibrium (NLTE) model, which takes into account deviations from both ionization equilibrium and equilibrium between electron and heavy-particle temperatures although assumes quasi-neutrality, then the boundary conditions must describe the near-electrode space-charge sheath. If the bulk plasma is described by means of a 2T model, which takes into account the temperature non-equilibrium but assumes ionization equilibrium and quasi-neutrality, then the boundary conditions must describe the space-charge sheath and the adjacent layer of quasi-neutral plasma where deviations from ionization equilibrium are localized (the so-called ionization layer). As shown in [3] for the plasma–cathode interaction, these two approaches give results close to each other and to results of straightforward numerical modelling.

On the other hand, most works dedicated to simulation of high-pressure arc discharges employ the assumption of local

[4] Authors to whom any correspondence should be addressed.

thermodynamic equilibrium (LTE). LTE models are significantly simpler than the NLTE and 2T models, requiring less work on formulation of boundary conditions and evaluation of transport coefficients, and do not involve kinetic coefficients. LTE models are also much simpler for numerical realization and, in principle, may be implemented by means of ready-to-use specialized software such as Plasimo [4] or the Equilibrium DC Discharge (sub)module of the Plasma module of COMSOL Multiphysics®. It is therefore highly desirable to develop a self-consistent joining of a numerical model of LTE bulk plasma with a cathode. The importance of this subject has been realized long ago and many attempts have been made; e.g. [5–12]. However, there is still no universally accepted approach. In fact, many researchers do not consider the physics of plasma–electrode interaction and employ the LTE equations right to the electrode surfaces. One of the problems of such an approach is an unrealistically high resistance of the near-electrode plasma, which requires some or other numerical cut-off; e.g. discussion in [13].

In this work, a self-consistent numerical-modelling joining of the LTE bulk plasma with a cathode is realized on the basis of the balance of energy in the near-cathode non-equilibrium plasma layer (the layer where deviations from the LTE are localized or, in other words, the layer separating the LTE bulk from the cathode surface), with the use of a numerical model of the space-charge sheath adjacent to the cathode surface and the ionization layer. The joining of the LTE bulk plasma with an anode is based on the balance of energy in the near-anode non-equilibrium plasma layer with the use of computations of the anode heating voltage [14].

The calculations are performed for the atmospheric-pressure arc in argon for a wide current range 20–200 A. The calculation results are compared with those obtained with the use of the 2T [15] and NLTE approaches [16] as well as with the experiment [17] and a good agreement is found.

The outline of the paper is as follows. The governing equations of the LTE arc bulk and the boundary conditions on the interfaces separating the bulk from the electrodes are given in section 2. Numerical results are given and discussed in section 3. The concluding remarks are summarized in section 4.

2. Numerical model

2.1. The bulk plasma

The calculation domain includes the LTE plasma bulk and the electrodes. The system of MHD equations describing the bulk plasma is well known and includes the Navier–Stokes equation, the equation of conservation of energy, the current continuity equation supplemented with Ohm's law, and the equation for vector potential. For the steady state and a subsonic laminar flow, this system of equations reads:

$$\nabla \cdot \rho \boldsymbol{u} = 0, \tag{1}$$

$$\nabla \cdot \rho \boldsymbol{u} \otimes \boldsymbol{u} = -\nabla p + \nabla \cdot \eta \left(\nabla \boldsymbol{u} + (\nabla \boldsymbol{u})^{\boldsymbol{T}} \right) - \frac{2}{3} \nabla (\eta \nabla \cdot \boldsymbol{u}) + \boldsymbol{j} \times \boldsymbol{B}, \tag{2}$$

$$\rho c_{\mathrm{p}} (\boldsymbol{u} \cdot \nabla T) + \nabla \cdot \boldsymbol{q} = -\boldsymbol{j} \cdot \nabla \varphi - Q_{\mathrm{rad}}, \tag{3}$$

$$\boldsymbol{q} = -\lambda \nabla T - \left(\frac{5}{2} + k_{\mathrm{T}} \right) \frac{kT}{e} \boldsymbol{j}, \tag{4}$$

$$\nabla \cdot \boldsymbol{j} = 0, \tag{5}$$

$$\boldsymbol{j} = \sigma \left(-\nabla \varphi + k_{\mathrm{T}} \frac{k}{e} \nabla T \right), \tag{6}$$

$$\nabla \times \frac{1}{\mu_0} \boldsymbol{B} = \boldsymbol{j}, \tag{7}$$

$$\boldsymbol{B} = \nabla \times \boldsymbol{A}. \tag{8}$$

Here $\boldsymbol{u}$, p, and T are the mean mass velocity, pressure and temperature of the plasma; $\boldsymbol{j}$, φ, $\boldsymbol{B}$, and $\boldsymbol{A}$ are the current density, the electrostatic potential, the self-induced magnetic field and vector potential; ρ, η, c_{p}, λ, k_{T}, and σ are the mass density, viscosity, specific heat at constant pressure, thermal conductivity, thermal-diffusion ratio and electrical conductivity of the plasma; the term Q_{rad} describes radiation losses; k and e are Boltzmann constant and elementary charge. Note that the second term on the right-hand side of equation (4) describes enthalpy transport by the electric current and the effect inverse to thermal diffusion. The second term in the parentheses on the right-hand side of equation (6) describes the thermal diffusion current.

Results reported in this paper refer to atmospheric-pressure argon plasma. Thermodynamic properties ρ, c_{p} and transport coefficients η, λ, σ have been taken from [18]. The thermal diffusion ratio k_{T} has been calculated by means of the data from [19]. The radiation loss term is evaluated according to [20].

2.2. The electrodes

The heat conduction and current continuity equations are solved in the electrodes:

$$\nabla \cdot (\lambda_s \nabla T) + \sigma_s (\nabla \varphi)^2 = 0, \tag{9}$$

$$\nabla \cdot (\sigma_s \nabla \varphi) = 0. \tag{10}$$

Here σ_s and λ_s are electrical and thermal conductivities of the electrode material. Results reported in this paper refer to the tungsten cathode and copper anode. Data on thermal conductivity of tungsten and copper are taken from [21] and the electrical conductivity is evaluated in terms of thermal conductivity with the use of the Wiedemann–Franz law.

2.3. Arc-electrode interfaces

The bulk LTE plasma is separated from each of the electrodes by a near-electrode plasma layer where deviations from LTE are localized (the non-equilibrium layer); see figure 1. These non-equilibrium layers are assumed to be thin and are not included into the computation domain; the relevant physics is taken into account through boundary conditions on the interfaces between the bulk plasma and the electrodes.

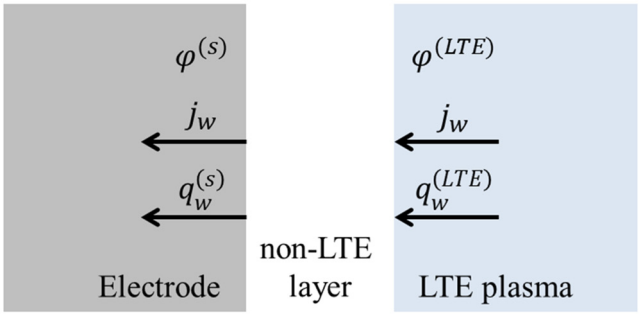

Figure 1. Schematic representation of the plasma–electrode interface.

Distributions of the temperature and electrostatic potential in the LTE bulk and in the electrodes are governed by elliptic differential equations, hence, two electric and two thermal boundary conditions are required at each interface. The electrostatic potential is discontinuous at the interface:

$$\varphi^{(\mathrm{LTE})} - \varphi^{(\mathrm{s})} = U, \tag{11}$$

where the upper indices LTE and s denote values on the LTE-plasma side of the interface and on the side of the electrode, respectively, and U is the near-electrode voltage drop, which in the general case varies along the electrode surface.

The electric current is continuous at the interface. In other words, the normal components of the densities of electric current from the LTE plasma to the near-electrode layer and from the electrode surface into the solid are equal. In the following, these densities are designated j_w; $j_w > 0$ for the cathode and $j_w < 0$ for the anode.

Of central importance is matching of temperature distributions. The appropriate boundary condition is the equation of balance of energy in the near-electrode layer:

$$q_w^{(\mathrm{nl})} - q_w^{(\mathrm{LTE})} = j_w U - \frac{j_w A_\mathrm{f}}{e}. \tag{12}$$

Here $q_w^{(\mathrm{LTE})}$ and $q_w^{(\mathrm{nl})}$ are normal components of the energy fluxes from the LTE bulk plasma to the near-electrode layer and from the near-electrode layer to the electrode surface, respectively, and A_f is the work function of the electrode material. The first term on the right-hand side of equation (12) represents the electric power per unit area of the near-electrode layer deposited by the arc power supply. The second term accounts for the energy necessary for extracting the electrons from metal, if $j_w > 0$ (i.e. on the cathode) and the energy released when the electrons pass from the plasma into metal, if $j_w < 0$ (on the anode).

Contributions of radiation emission and absorption in the near-electrode layer to the energy balance of the layer are neglected. Accordingly, the energy flux densities $q_w^{(\mathrm{LTE})}$ and $q_w^{(\mathrm{nl})}$ are evaluated with account of energy transported by the plasma species but not of the radiation energy transport; in particular, $q_w^{(\mathrm{LTE})}$ is given by equation (4). On the other hand, thermal balance of the electrodes may be significantly affected by the cooling of the electrode surface by radiation. Therefore, $q_w^{(\mathrm{nl})}$ does not coincide with $q_w^{(\mathrm{s})}$ the normal component of the flux of energy removed from the electrode surface by thermal conduction into the solid. In fact, $q_w^{(\mathrm{nl})} = q_w^{(\mathrm{s})} + q^{(\mathrm{rad})}$, where $q^{(\mathrm{rad})}$ is the density of net energy flux removed from the electrode surface by radiation into the plasma. In this work, $q^{(\mathrm{rad})}$ is evaluated in terms of emissivities of tungsten and copper taken from [22] and [23], respectively.

Note that equation (12) represents an analogue of equation (A.5) of [3] except that the latter contains a term accounting for the energy released at the solid surface due to neutralization of the ions coming from the plasma. The reason for this difference is as follows: equation (12) refers to the near-electrode layer on the whole (and not to only the space-charge sheath, as equation (A.5) [3] does), and the contribution to this equation of the energy released at the surface due to neutralization of the ions coming from the plasma is compensated by the energy consumed for generation of the ion flux in the quasi-neutral part of the non-equilibrium layer.

The second thermal boundary condition at the interface needs to be specified. One more boundary condition is needed since the distribution of the near-electrode voltage drop U along the electrode surface remains indeterminate up to now. The two lacking boundary conditions describe the specific physics of the near-electrode layer and are therefore different for the cathode and the anode.

As far as the plasma–cathode interface is concerned, the use will be made of the fact that a significant power is deposited into the near-cathode layer by the arc power supply; a part of this power is transported to the cathode surface, thus heating it to temperatures sufficient for electron emission, and the rest is transported into the bulk plasma. As a consequence, the plasma–cathode interaction is governed primarily by processes in the near-cathode layer and is to the first approximation independent of processes in the arc bulk. The latter has been confirmed by the numerical modelling; see [3], section 4.

The current transfer across the near-cathode layer is locally 1D and governed by local values of the cathode surface temperature T_w and near-cathode voltage drop U. (In principle, j_w may be considered as a control parameter instead of U, however this would be less convenient.) After the 1D current transfer across the near-cathode layer has been computed, one will know the densities of energy flux and electric current, directed from the near-cathode layer to the cathode surface, as functions of T_w and U. Let us designate these functions $f_1(T_w, U)$ and $f_2(T_w, U)$, respectively. Then one can formulate the two lacking boundary conditions as

$$q_w^{(\mathrm{nl})} = f_1(T_w, U), j_w = f_2(T_w, U). \tag{13}$$

One needs to invoke a model of 1D current transfer across the near-cathode layer in order to evaluate functions $f_1(T_w, U)$ and $f_2(T_w, U)$. For example, one can resort to the unified modelling of near-cathode non-equilibrium plasma layers of high-pressure arc discharges [24]. A simpler option is to use a model based on dividing the non-equilibrium plasma layer into zones dominated by different physical processes. These zones include the space-charge sheath, the ionization layer, and a layer where deviations between electron and heavy-particle temperatures are localized (the layer of thermal

non-equilibrium). The most important zones are the space-charge sheath, which is where the most of electrical power is deposited, and the ionization layer, which is where the ion flux to the cathode surface is formed; e.g. [25]. Models of near-cathode layers of high-pressure arc discharges based on treatment of these two zones in some or other approximations were developed in [26–31]. In this work, functions $f_1(T_w, U)$ and $f_2(T_w, U)$ are computed by means of the model [27] (a summary of equations of this model can be found in [32]). Note that the recent comparison [3] has shown that results given by this model agree in a wide arc current range with results given by the more complex model [16].

The two lacking boundary conditions at the plasma–anode interface are obtained by assuming that the density of energy flux transported by the plasma species from the near-anode layer to the anode surface is proportional to the local current density and by neglecting the voltage drop in the near-anode layer:

$$q_w^{(\mathrm{nl})} = -j_w U_\mathrm{h}, U = 0. \quad (14)$$

Here U_h is a constant coefficient called the anode heating voltage or volt equivalent of the anodic heat flux. The anode heating voltage was derived in [14] from a detailed numerical modelling of near-anode layers in high-pressure arc discharges in several gases in a wide range of current densities, anode surface temperatures and plasma pressures. For the atmospheric-pressure argon plasma in the range of j_w of interest to this work, U_h may be set equal to 6 V.

2.4. Boundary conditions

Two slightly different axially symmetric geometries have been considered in this work. The geometry 1, which corresponds to conditions of experiment [17], is shown in figure 2. The cathode represents a tungsten rod at a length of 12 mm with a hemispherical tip of 1 mm radius. The geometry 2 corresponds to the conditions of the experiment [33]: the cathode represents a rod made of thoriated tungsten at a radius of 1.6 mm with the conical tip with an angle of 60°. Different cathode lengths in the range from 10 to 20 mm are investigated. In both geometries, the anode is flat, made of copper, and has diameter of 60 mm. The gap between the cathode and the anode is 10 mm.

The equations formulated in section 2.1 are solved in the domain ACDEH and those formulated in section 2.3 are solved in the domains ABC and HEFG. The matching conditions formulated in section 2.3 and the no-slip conditions for the mean mass velocity are applied on the boundaries AC and EH.

The temperature on BCD and EFG is set equal to 300 K. The normal component of the current density vanishes on CDE. The electrostatic potential is zero on EFG. An arbitrary constant value of potential is assumed at the cathode base BC. In principle, this value may be considered as a prescribed control parameter (the arc voltage with the opposite sign). However, we will consider the arc current I as a control parameter and the value of potential at the cathode base as a parameter to be found.

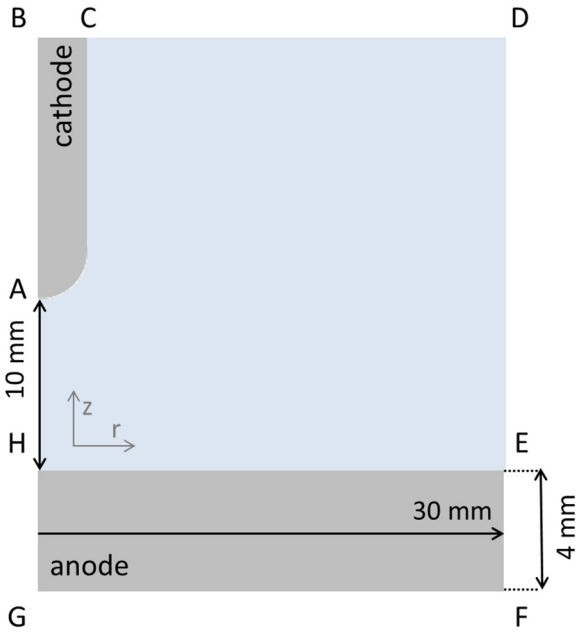

Figure 2. Schematic view of the computational domain.

On DE, the temperature is set equal to 300 K for geometry 1 and the normal derivative of the temperature vanishes for geometry 2. On CD, the no-slip condition is applied for geometry 1 and the normal stress is set equal to zero for geometry 2. On DE, the normal stress vanished for geometry 1 and pressure is 1 atm for geometry 2.

2.5. The workflow

Numerical modelling [32] has shown that the voltage drop in the near-cathode layer is approximately the same at all points of the cathode surface inside the arc attachment. This may be exploited in order to simplify the workflow: if U is assumed constant, then the problem in the cathode is decoupled from the rest of the equations and may be solved independently.

The procedure is as follows. At the first step, functions $f_1(T_w, U)$ and $f_2(T_w, U)$ are evaluated by means of the model [27]. At the second step, equations (9) and (10) are solved in the cathode with the above-described boundary conditions. The additional condition, which governs the near-cathode voltage U, is that the arc current, evaluated as the integral of the function f_2 over the cathode surface, takes the prescribed value I. After this problem has been solved for a given value of I, one will know distributions of temperature and (to the accuracy of an additive constant) electrostatic potential in the cathode. In particular, one will know distributions of $q_w^{(\mathrm{s})}$ and j_w over the cathode surface for this I. The above-described procedure of the calculation of the cathodic part of the arc coincides with the so-called model of nonlinear surface heating [25]; and references therein.

Thus, at this stage one will know j_w on the plasma–cathode interface AC as a function of position, and $q_w^{(\mathrm{LTE})}$ may be

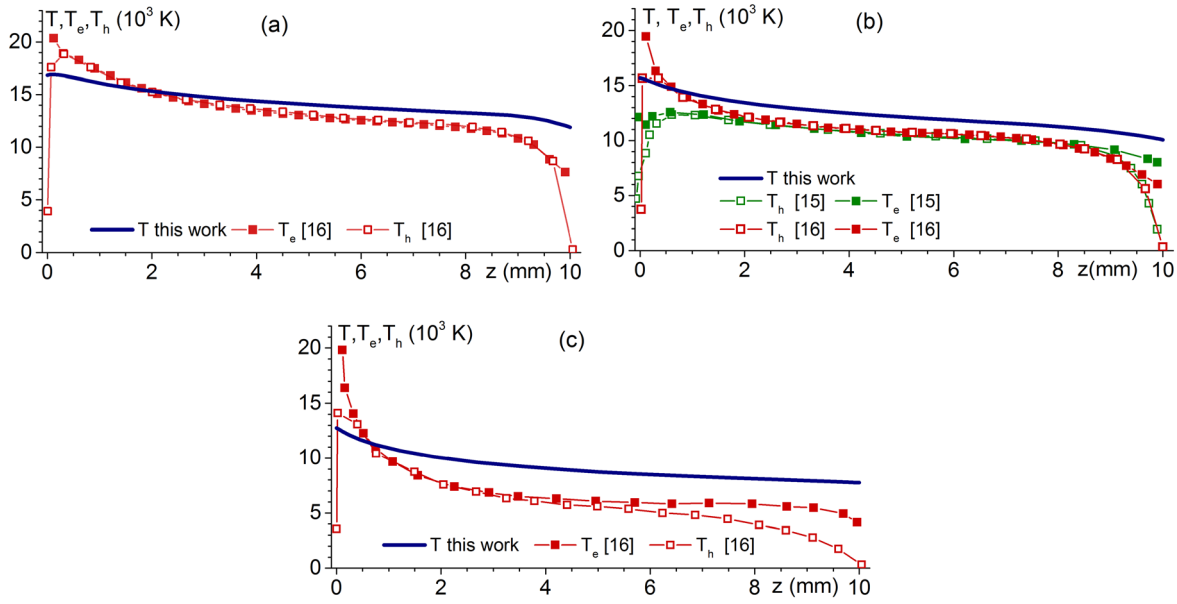

Figure 3. Distributions of temperatures given by different models along the arc axis.

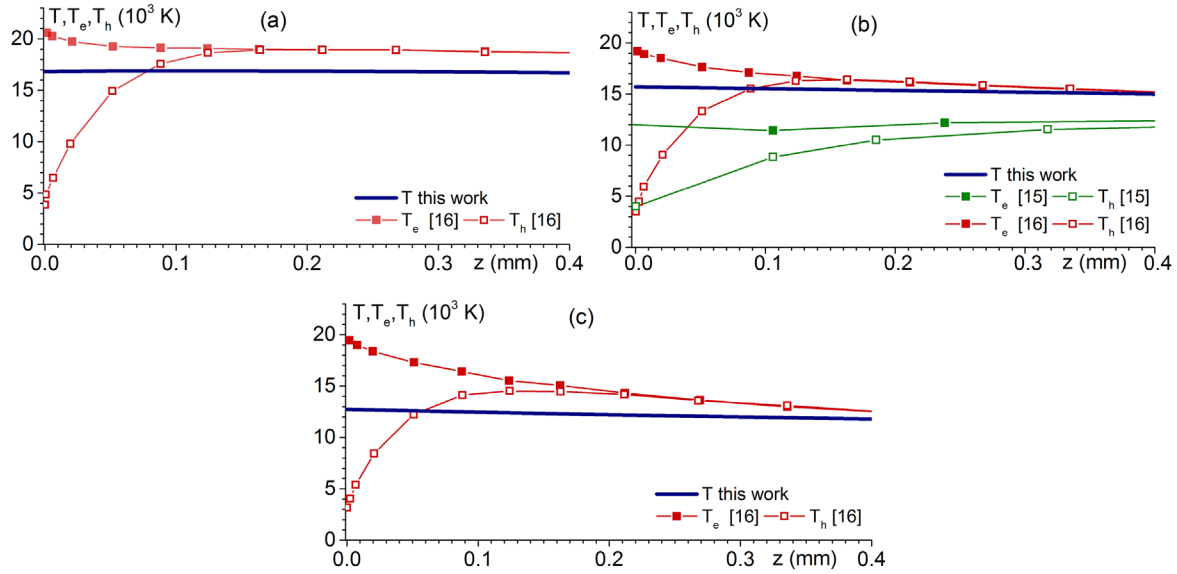

Figure 4. Details of distributions of temperatures given by different models on the arc axis in the vicinity of the cathode.

evaluated from equation (12). At the third step, equations (1)–(8), governing the bulk LTE plasma, are solved jointly with equations (9)and (10) in the anode, using known distributions of $q_w^{(\mathrm{LTE})}$ and j_w on the plasma–cathode interface AC as boundary conditions for equations (3) and (5). After that, one finds the additive constant in the distribution of electrostatic potential in the cathode by applying equation (11) on the axis of symmetry, and thus the arc voltage.

The solution is complete for the arc current I being considered. Note that equation (11) has been satisfied only at one point of the cathode surface (on the axis of symmetry). This is a price to be paid for simplifying the procedure by assuming U constant. However, the modelling results show that $\varphi^{(\mathrm{LTE})}$ does not vary much on the cathode surface inside the arc attachment; the voltage drop inside the cathode is small, meaning that $\varphi^{(\mathrm{s})}$ varies little as well; hence, the residual in equation (11) is not large.

Commercial software COMSOL Multiphysics (version 5.2) is used for numerical calculations. The 'Heat transfer in solids' and 'Electrical currents' modules are used for solving the equations in the electrodes. The module 'Equilibrium DC Discharge' is used in the bulk LTE plasma. The stationary fully coupled solver with direct computation based on MUMPS (MUltifrontal Massively Parallel Sparse solver) was used. The relative tolerance was set equal to 10^{-3}. The number of degrees of freedom solved was relatively small (around 10 000 including the bulk plasma domain and the electrodes), so the code was quite fast.

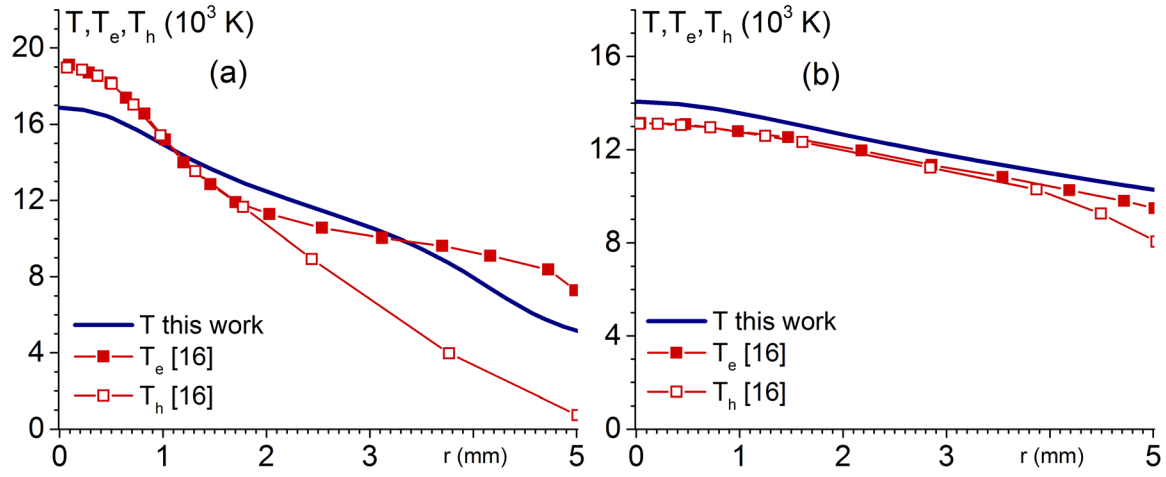

Figure 5. Radial distributions of temperatures in the arc column at different distances from the cathode tip. $I = 200$ A.

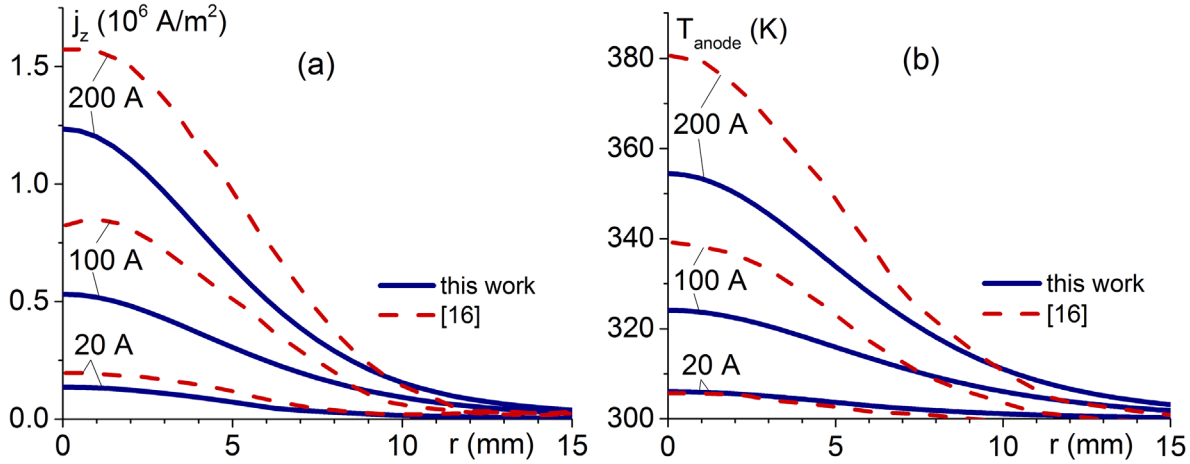

Figure 6. Distributions of the current density (a) and the surface temperature (b) along the anode surface given by different models.

3. Results

3.1. Tungsten cathode with a hemispherical tip

The aim of this section is to compare the results given by the model of this work with those given by the (more involved) 2T [15] and NLTE [16] models and with the experimental data. As mentioned above, the cathodic part of the arc in the framework of the approach of this work (as well as the approach [15]) is described by the model of nonlinear surface heating. A detailed comparison of results given by the latter with those of [16] has been performed in [3] and a good agreement was found. Therefore, here we compare parameters of the arc column and the anode.

Distributions along the arc axis of the plasma temperature T computed in this work and of the heavy-particle and electron temperatures T_h and T_e, given by the 2T and NLTE models, are compared in figure 3 for currents 200, 100, 20 A. Details of the distributions in the vicinity of the cathode are shown in figure 4. The agreement in the arc bulk is reasonably good for $I = 200$ and 100 A and not so good for $I = 20$ A, where deviations from LTE in the bulk become significant. On the other hand, there are significant deviations between T and T_h near the electrodes. This is the central point of the proposed approach: the fast decrease of the heavy-particle temperature in the near-electrode regions is described not by a solution of the LTE bulk equations but rather through the boundary conditions on the interfaces between the LTE plasma and the electrodes.

Distributions of the temperatures in the radial direction at 0.2 mm from the cathode tip and in the midplane of the arc are shown in figure 5 for the arc current of 200 A. Again, the agreement is reasonably good.

Distributions along the anode surface of the axial current density and the anode surface temperature computed in this work are compared with those given by the NLTE model in figure 6 for arc currents 200, 100 and 20 A. The temperature

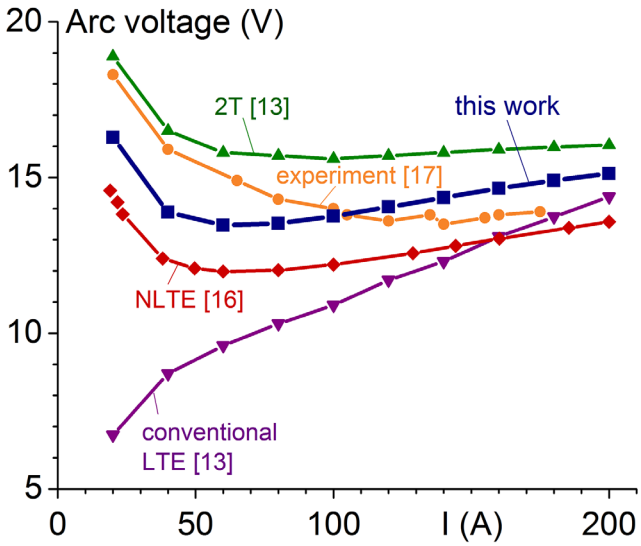

Figure 7. Arc voltage evaluated by means of different models and the experimental data.

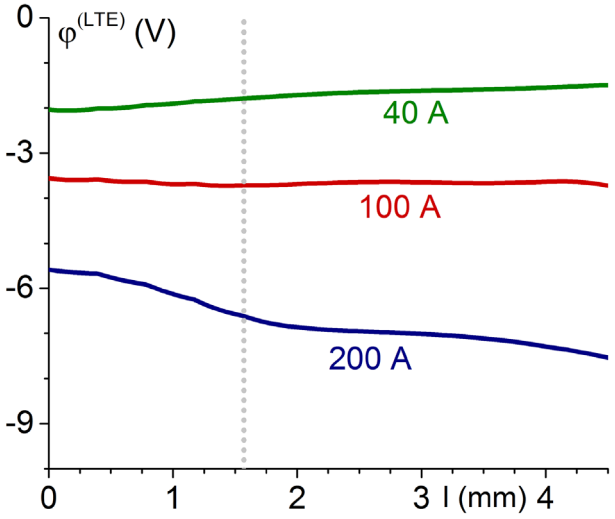

Figure 8. Distribution of electrostatic potential in the LTE arc column evaluated at the plasma–cathode interface.

of the anode surface does not exceed 360 K, even for arc current of 200 A, due to intensive external cooling. The agreement between the two models is good.

In the framework of the model of this work, the total arc voltage is obtained by adding up the voltage drops inside the electrodes, the voltage drop in the LTE arc bulk, and the near-cathode voltage drop U. The current–voltage characteristic (CVC) of the arc, evaluated in this way for a wide current range, is shown in figure 7. (Note that the voltage drop inside the electrodes is negligible in these conditions.) Also shown are data from the NLTE and 2T models, as well as the data from the experiment [17] referring to the diffuse cathode arc attachment. The CVCs given by the NLTE and 2T models and the model of this work agree with each other and with the experiment reasonably well in the whole range of arc currents from 20 to 175 A.

Also shown in figure 7 is the CVC evaluated in the framework of the conventional LTE model, i.e. without an account of near-electrode layers. This CVC is of a different character than the ones given by all the other theoretical models and the experimental one: the arc voltage monotonically increases for all currents. Comparing with the model of this work, one can conclude that the different character stems from the neglect of the near-electrode layers in the conventional LTE model, rather than from the mere fact that deviations from LTE become more pronounced as I decreases. Another difference between the model of this work and the conventional LTE model is that the former does not require any cut-off in evaluation of the resistance of the near-electrode plasma and therefore poses no limitations on the step of numerical mesh near the electrodes.

Distribution of electrostatic potential in the LTE arc column evaluated at the plasma–cathode interface is shown in figure 8. Here, l is the distance measured along the generatrix of the cathode surface from the centre of the tip (i.e. from point A in figure 2) and the vertical dashed line designates the end of the spherical tip. The variation of potential $\varphi^{(\mathrm{LTE})}(l)$ in the region $l < 4$ mm, where the arc is attached to the cathode, is not large. Hence, the voltage drop in the near-cathode layer does not change much from one point of the arc attachment to the other. This supports the corresponding assumption made in order to simplify the workflow (section 2.5) and to avoid more complex computations similar to those [16, 31].

3.2. Thoriated-tungsten cathode with a conical tip

Since the exact cathode geometry was not specified in [33], calculations for the experimental conditions [33] have been performed for several variants of geometry for the arc current of 100 A. The distributions of temperature on the arc axis are shown in figure 9 for the cathode length h varying in the range from 15 to 20 mm. One can see that an increase in h causes an appreciable decrease of the plasma temperature near the cathode tip. This may be understood as follows. Higher thermal resistance of a cathode is favourable for wider attachments of the arc to the cathode; an effect well familiar to designers of arc lamps. Hence, an increase of h causes a decrease of the current density at the cathode tip and, consequently, lower plasma temperatures near the tip.

Results of computations for a cathode with a flat front, i.e. a plateau at the (conical) tip of the cathode, are shown in figure 10. Here r_0 is the radius of the plateau; note that $r_0 = 0$ corresponds to the sharp conical tip to which figure 9 refers. The cathode length was 15 mm in these calculations. An increase in r_0 causes a decrease of the plasma temperature near the tip, which is again a consequence of decrease of the current density at the cathode surface.

Thus, the modelling has revealed a significant impact produced by the details of the cathode geometry over the distribution of the current density along the cathode surface and therefore over the plasma temperature; an interesting and potentially important effect that deserves further attention.

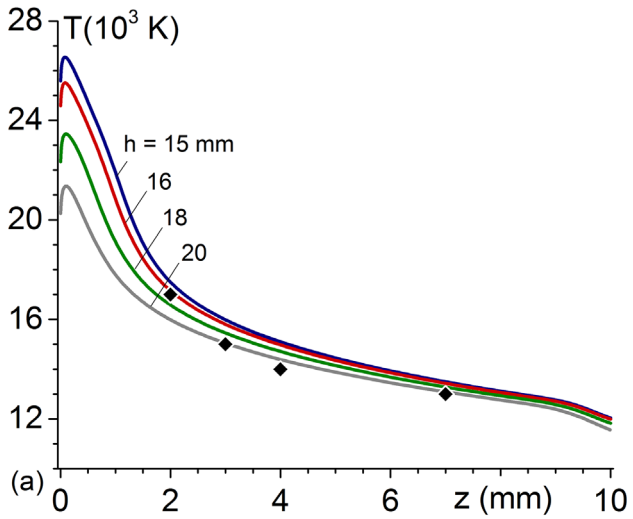

Figure 9. Lines: computed distributions of temperature along the arc axis for cathodes of different lengths. Diamonds: experiment [33]. $I = 100$ A.

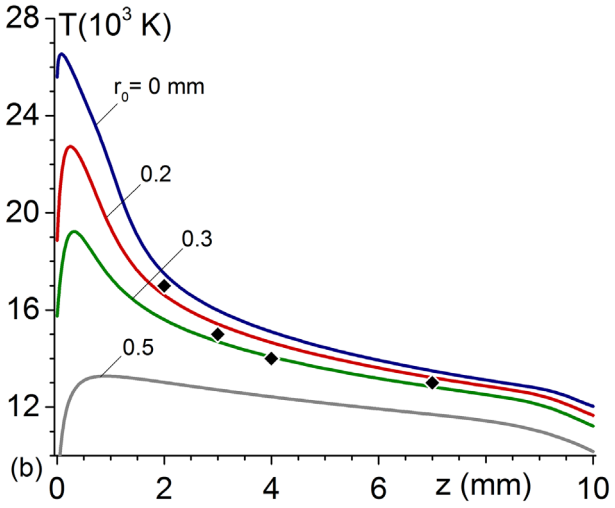

Figure 10. Lines: computed distributions of temperature along the arc axis for cathodes with different plateau radii. Diamonds: experiment [33]. $I = 100$ A.

4. Conclusions

The standard approach to simulation of high-pressure arc discharges is to use the system of magneto-hydrodynamic equations written in the LTE approximation. Such models are significantly simpler than the two-temperature (2T) and fully non-equilibrium (NLTE) models; their numerical realization is simpler than well and may rely on ready-to-use specialized software. However, one needs to find a way of matching of the LTE model of the bulk plasma with the electrodes that would reasonably accurately reflect the physics of the plasma–electrode interaction. In this work, this matching is realized with the use of equations of balance of energy in the non-equilibrium near-electrode layers that separate the LTE bulk plasma and the electrodes.

As an example, numerical simulation of a free-burning arc in atmospheric-pressure argon plasma is reported in the current range from 20 to 200 A. The simulation results are compared with those given by the (more sophisticated) 2T and NLTE models and with the experiment. The agreement in the arc bulk is reasonably good for arc currents of 100 A or higher and is not so good for lower currents, where deviations from LTE in the bulk become significant. On the other hand, there are significant deviations between the plasma temperature given by the model of this work and the heavy-particle temperature given by the 2T and NLTE models near the electrodes. This is the central point of the proposed approach: the fast decrease of the heavy-particle temperature in the near-electrode regions is described not by a solution of the LTE bulk equations but rather through the boundary conditions on the interfaces between the LTE plasma and the electrodes.

The arc voltage, given by the model of this work, agrees reasonably well with the values given by the 2T and NLTE models and with the experiment in the whole range of arc currents from 20 to 175 A, in contrast to the arc voltage given by the conventional LTE model (the one that disregards the near-electrode layers). Another difference between the model of this work and the conventional LTE model is that the present model does not require a cut-off in evaluation of the resistance of the near-electrode plasma and therefore poses no limitations on the step of numerical mesh near the electrodes.

The approach proposed in this work allows one to develop models that are, on one hand, physically justified and therefore applicable to a wide range of conditions, and on the other hand, fast and robust. In particular, a simple 2D model reported in this work has predicted a strong effect produced by details of the cathode geometry over the distribution of the current density along the cathode surface and therefore over the plasma temperature; a result that seems to be interesting and potentially important and therefore worth further numerical modelling and experimental verification.

It is well known that the model of nonlinear surface heating under certain conditions admits multiple steady-state solutions, existing for the same arc current and describing the diffuse mode of current transfer to the cathode and mode(s) with spots; e.g. [25], and references therein. The proposed approach allows one to simulate the effect produced by different modes of current transfer to the cathode over the bulk plasma. This simulation is beyond the scope of this work, however it is of significant theoretical and industrial interest and may be undertaken in the future.

Acknowledgments

The work at Université d'Orléans was supported by Zodiac aerospace and the work at Universidade da Madeira was supported by FCT—Fundação para a Ciência e a Tecnologia of Portugal through the project Pest-OE/UID/FIS/50010/2013. The authors thank Yann Cressault for providing data on some transport coefficients of the plasma.

References

[1] Murphy A B 2015 A perspective on arc welding research: the importance of the arc, unresolved questions and future directions *Plasma Chem. Plasma Process* **35** 471–89

[2] Gleizes A 2015 Perspectives on thermal plasma modelling *Plasma Chem. Plasma Process* **35** 455–69

[3] Benilov M S, Almeida N A, Baeva M, Cunha M D, Benilova L G and Uhrlandt D 2016 Account of near-cathode sheath in numerical models of high-pressure arc discharges *J. Phys. D: Appl. Phys.* **49** 215201

[4] van Dijk J, Peerenboom K, Jimenez M, Mihailova D and van der Mullen J 2009 The plasma modelling toolkit Plasimo *J. Phys. D: Appl. Phys.* **42** 194012

[5] Zhu P, Lowke J J and Morrow R 1992 A unified theory of free burning arcs, cathode sheaths and cathodes *J. Phys. D: Appl. Phys.* **25** 1221

[6] Lowke J J, Morrow R and Haidar J 1997 A simplified unified theory of arcs and their electrodes *J. Phys. D: Appl. Phys.* **30** 2033

[7] Sansonnens L, Haidar J and Lowke J J 2000 Prediction of properties of free burning arcs including effects of ambipolar diffusion *J. Phys. D: Appl. Phys.* **33** 148

[8] Lowke J J and Tanaka M 2008 The physics of non-thermionic cathodes of electric arcs *Proc. 17th Int. Conf. on Gas Discharges and Their Applications (Cardiff, UK)* pp 137–40

[9] Cayla F, Freton P and Gonzalez J J 2008 Arc/cathode interaction model *IEEE Trans. Plasma Sci.* **36** 1944–54

[10] Gonzalez J J, Cayla F, Freton P and Teulet P 2009 Two-dimensional self-consistent modelling of the arc/cathode interaction *J. Phys. D: Appl. Phys.* **42** 145204

[11] Alaya M, Chazelas C, Mariaux G and Vardelle A 2015 Arc-cathode coupling in the modeling of a conventional DC plasma spray torch *J. Therm. Spray Technol.* **24** 3–10

[12] Shirvan A J and Choquet I 2016 A review of cathode-arc coupling modeling in GTAW *Weld. World* **60** 821–35

[13] Benilov M S, Benilova L G, Li H-P and Wu G-Q 2012 Sheath and arc-column voltages in high-pressure arc discharges *J. Phys. D: Appl. Phys.* **45** 355201

[14] Almeida N A, Cunha M D and Benilov M S 2017 Computing anode heating voltage in high-pressure arc discharges and modelling rod electrodes in dc and ac regimes *J. Phys. D: Appl. Phys.* (submitted)

[15] Li H-P and Benilov M S 2007 Effect of a near-cathode sheath on heat transfer in high-pressure arc plasmas *J. Phys. D: Appl. Phys.* **40** 2010

[16] Baeva M, Benilov M S, Almeida N A and Uhrlandt D 2016 Novel non-equilibrium modelling of a DC electric arc in argon *J. Phys. D: Appl. Phys.* **49** 245205

[17] Mitrofanov N K and Shkol'nik S M 2007 Two forms of attachment of an atmospheric-pressure direct-current arc in argon to a thermionic cathode *Tech. Phys.* **52** 711–20

[18] Devoto R S 1973 Transport coefficients of ionized argon *Phys. Fluids* **16** 616

[19] Cressault Y 2016 private communication

[20] Erraki A 1999 Etude du transfert radiatif dans les plasmas thermiques: application au SF6 et au mélange Argon-Fer *PhD Thesis* University Paul Sabatier, Toulouse, France

[21] Touloukian Y S, Powell R W, Ho C Y and Klemens P G 1970 *Thermophysical Properties of Matter—The TPRC Data Series. Volume 1. Thermal Conductivity—Metallic Elements and Alloys* (*Thermophysical Properties of Matter*) vol 1 (New York: Plenum)

[22] Yih S W H and Wang C T 1979 *Tungsten : Sources, Metallurgy, Properties, and Applications* (New York: Plenum)

[23] Window B and Harding G 1981 Thermal emissivity of copper *J. Opt. Soc. Am.* **71** 354–7

[24] Almeida N A, Benilov M S and Naidis G V 2008 Unified modelling of near-cathode plasma layers in high-pressure arc discharges *J. Phys. D: Appl. Phys.* **41** 245201

[25] Benilov M S 2008 Understanding and modelling plasma–electrode interaction in high-pressure arc discharges: a review *J. Phys. D: Appl. Phys.* **41** 144001

[26] Benilov M S and Marotta A 1995 A model of the cathode region of atmospheric pressure arcs *J. Phys. D: Appl. Phys.* **28** 1869

[27] Benilov M S and Cunha M D 2002 Heating of refractory cathodes by high-pressure arc plasmas: I *J. Phys. D: Appl. Phys.* **35** 1736

[28] Schmitz H and Riemann K-U 2002 Analysis of the cathodic region of atmospheric pressure discharges *J. Phys. D: Appl. Phys.* **35** 1727

[29] Lichtenberg S, Dabringhausen L, Langenscheidt O and Mentel J 2005 The plasma boundary layer of HID-cathodes: modelling and numerical results *J. Phys. D: Appl. Phys.* **38** 3112

[30] Chen T, Wang C, Liao M-R and Xia W-D 2016 Diffuse and spot mode of cathode arc attachments in an atmospheric magnetically rotating argon arc *J. Phys. D: Appl. Phys.* **49** 085202

[31] Chen T, Wang C, Zhang X-N, Zhang H and Xia W-D 2017 Thermal and electrical influences from bulk plasma in cathode heating modeling *Plasma Sources Sci. Technol.* **26** 025002

[32] Benilov M S, Cunha M D and Naidis G V 2005 Modelling interaction of multispecies plasmas with thermionic cathodes *Plasma Sources Sci. Technol.* **14** 517

[33] Hsu K C, Etemadi K and Pfender E 1983 Study of the free-burning high-intensity argon arc *J. Appl. Phys.* **54** 1293–301